Received: 9 June 2020 | Revised: 19 October 2020 | Accepted: 1 November 2020

DOI: 10.1002/humu.24139

RESEARCH ARTICLE

Human Mutation HGVS HUMAN GENOME VARIATION SOCIETY WILEY

Biallelic *TMEM251* variants in patients with severe skeletal dysplasia and extreme short stature

Noor U. Ain[1,2] | Niaz Muhammad[1] | Mehdi Dianatpour[3,4] | Marta Baroncelli[5] | Muddassar Iqbal[1] | Mohammad A. F. Fard[6] | Ihtisham Bukhari[1] | Sufian Ahmed[1] | Massoumeh Hajipour[6] | Zahra Tabatabaie[6] | Hamidreza Foroutan[7] | Ola Nilsson[5,8] | Mohammad A. Faghihi[6] | Outi Makitie[2,9,10] | Sadaf Naz[1]

[1]School of Biological Sciences, University of the Punjab, Lahore, Pakistan

[2]Department of Molecular Medicine and Surgery and Center for Molecular Medicine, Karolinska Institutet, Stockholm, Sweden

[3]Department of Medical Genetics, School of Medicine, Shiraz University of Medical Sciences, Shiraz, Iran

[4]Stem Cell Technology Research Center, Shiraz University of Medical Sciences, Shiraz, Iran

[5]Division of pediatric endocrinology and Center for Molecular Medicine, Department of Women's and Children's Health, Karolinska Institutet and University Hospital, Stockholm, Sweden

[6]Persian BayanGene Research and Training Center, Shiraz, Iran

[7]Laparoscopy research center, Shiraz University of Medical Sciences, Shiraz, Iran

[8]School of Medical Sciences, Örebro University and Örebro University Hospital, Örebro, Sweden

[9]Children's Hospital, University of Helsinki and Helsinki University Hospital, Helsinki, Finland

[10]Folkhälsan Institute of Genetics, Helsinki, Finland

Correspondence
Sadaf Naz, School of Biological Sciences, University of the Punjab, Lahore, Pakistan.
Email: naz.sbs@pu.edu.pk

Outi Makitie, Children's Hospital, University of Helsinki and Helsinki University Hospital, Helsinki, Finland.
Email: outi.makitie@helsinki.fi

Present address
Noor U. Ain, Institute of Biomedical and Genetic Engineering, Islamabad, Pakistan.

Niaz Muhammad, Shaanxi Normal University, China.

Funding information
Academy of Finland; Forskningsrådet om Hälsa, Arbetsliv och Välfärd; National Institute for Medical Research Development, Grant/Award Number: 940714; Higher Eductation Comission Pakistan, Grant/Award Number: IRSIP; Koshish Foundation, USA; Sigrid Jusélius Foundation

Abstract

Skeletal dysplasias are a heterogeneous group of disorders ranging from mild to lethal skeletal defects. We investigated two unrelated families with individuals presenting with a severe skeletal disorder. In family NMD02, affected individuals had a dysostosis multiplex-like skeletal dysplasia and severe short stature (<−8.5 SD). They manifested increasingly coarse facial features, protruding abdomens, and progressive skeletal changes, reminiscent of mucopolysaccharidosis. The patients gradually lost mobility and the two oldest affected individuals died in their twenties. The affected child in family ID01 had coarse facial features and severe skeletal dysplasia with clinical features similar to mucopolysaccharidosis. She had short stature, craniosynostosis, kyphoscoliosis, and hip-joint subluxation. She died at the age of 5 years. Whole-exome sequencing identified two homozygous variants c.133C>T; p.(Arg45Trp) and c.215dupA; p.(Tyr72Ter), respectively, in the two families, affecting an evolutionary conserved gene *TMEM251* (NM_001098621.1). Immunofluorescence and confocal studies using human osteosarcoma cells indicated that TMEM251 is localized to the Golgi complex. However, p.Arg45Trp mutant TMEM251 protein was targeted less efficiently and the localization was punctate. *Tmem251* knockdown by small interfering RNA induced dedifferentiation of rat

Noor U. Ain, Niaz Muhammad, Mehdi Dianatpour, Outi Makitie, and Sadaf Naz contributed equally to this study.

primary chondrocytes. Our work implicates *TMEM251* in the pathogenesis of a novel disorder and suggests its potential function in chondrocyte differentiation.

KEYWORDS

Facial dysmorphology, Golgi, Iran, mucolipidosis, mucopolysaccharidosis, Pakistan

1 | INTRODUCTION

Skeletal dysplasias are a heterogeneous group of inherited disorders, usually of a monogenic etiology. They affect skeletal development and lead to variable skeletal anomalies, often accompanied by short stature (Krakow, 2015; Mortier et al., 2019). These disorders can be inherited in an autosomal recessive, autosomal dominant, X-linked recessive or X-linked dominant manner. Some skeletal disorders are associated with a spectrum of metabolic disturbances and extra-skeletal manifestations in the context of complex syndromes. The manifestations can include but are not limited to hepatosplenomegaly, cardiomyopathy, and pulmonary dysfunction (Longo et al., 2013; Saenger et al., 2007). Many of the metabolic disturbances observed in this group of disorders arise from perturbations of pathways involving modifications of proteins and lipids (Sparks & Krasnewich, 2017). These modifications are important for the stability or function of molecules including proteins that function in several tissues including cartilage and bone (Stanley, 2011). For example, many skeletal disorders with prominent extra-skeletal manifestations involve defects in glycosylation (Coman et al., 2008; Kranz et al., 2007).

Several metabolic disorders with severe skeletal consequences have been identified and delineated. These include lysosomal storage disorders, mucopolysaccharidosis (MIM# 309900; 253200; 25300), and mucolipidosis (MIM# 252600; 252605) among many others. So far, variants in genes encoding proteins participating in various cellular processes have been identified to cause skeletal dysplasia. Some of these proteins have an enzymatic role. For example, GALNS (MIM# 612222) is defective in mucopolysaccharidosis IV while GNPTAB (MIM# 607840) dysfunction is reported in mucolipidosis II/III. Other proteins with important functions in skeletal formation have structural roles. For example, collagen type X chain α1 (MIM# 120110) defects cause metaphyseal chondrodysplasia, Schmid type (MIM# 156500), and those disrupting Centromeric protein J (MIM# 609279) result in Seckel syndrome.

Mucopolysaccharidoses and mucolipidosis are lysosomal storage disorders that result from deficiency or erroneous function of any of the 11 enzymes required for the metabolism of glycosaminoglycans (GAGs) or from deficiency of *N*-acetylglucosamine-1-phosphotransferase (MIM# 607840), respectively. These disorders have several overlapping clinical features. These include facial dysmorphism, bone dysplasia, cardiac myopathy, joint deterioration, hepatosplenomegaly, impaired cognition, developmental regression, and in some cases, a reduced life expectancy (Ballabio & Gieselmann, 2009; Eklund & Freeze, 2006).

Although the molecular bases of many skeletal disorders are known, a significant number of others remain to be elucidated. In this study, we explored the genetics of severe skeletal dysplasia in individuals from Pakistan and Iran. Patients in both families had some features similar to mucopolysaccharidosis.

2 | MATERIAL AND METHODS

2.1 | Editorial policies and ethical considerations

The research on human subjects was approved by the Institutional Review Board of School of Biological Sciences, University of the Punjab, Lahore, Pakistan, and the ethics committee of Persian Bayangene Research and Training Institute, Shiraz, University of Medical Sciences, Iran. All participants or the parents of minor children provided written informed consent. Animals were handled according to the protocol approved by the Bioethical Committee of School of Biological Sciences, University of the Punjab, Lahore, Pakistan, and Bioethical Committee of Karolinska Institutet, Stockholm, Sweden.

2.2 | Subjects

We identified two consanguineous families NMD02 and ID01 (BY0084) (Figure 1), in which affected individuals had a mucolipidosis II α/β like syndrome (MIM# 252500). Clinical analyses involved complete blood counts and radiographs for two affected individuals III:9 and III:11 of family NMD02 and affected child IV:5 of ID01. Morning urine samples were collected from three affected III:9, III:10, III:11, and two unaffected individuals II:3, III:3 of family NMD02 for qualitative measurements of GAG levels by Berry spot test. Briefly, the urine sample was applied to a filter paper and air-dried. Then, toluidine blue O was applied and the development of purple color was regarded as the presence of GAGs in the urine. Lysozyme enzymes from dried blood were measured for individual IV:5 of family ID01. Blood samples were collected from all participants for genetic studies and the DNA was extracted by a standard protocol.

2.3 | Molecular analyses

For family NMD02, fluorescently labeled microsatellite markers located close to the respective genes (Table S1) were genotyped to exclude linkage of the disorder to *GNPTAB* (MIM# 607840), *GNPTG*

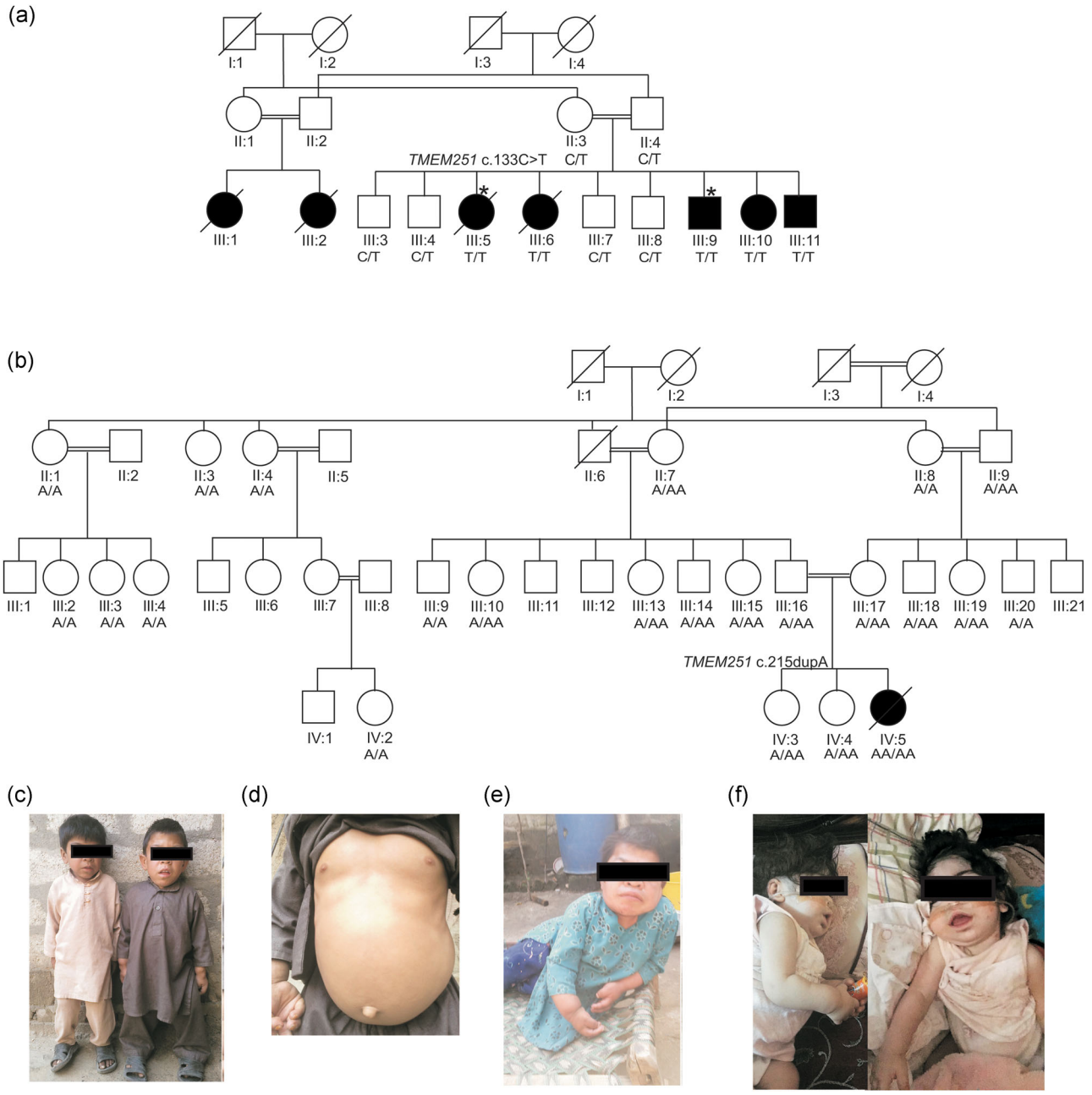

FIGURE 1 Pedigrees for NMD02 and ID01 and segregation of identified variants. (a) Pedigree of family NMD02 from Pakistan. Black symbols denote individuals affected with the disorder while open symbols represent the unaffected individuals. Strikethrough denotes deceased individuals. Genotypes for the *TMEM251* variant c.133C>T; p.(Arg45Trp) of all participants are shown under the respective symbols. Asterisks mark the individuals whose samples were subjected to exome sequencing. (b) Pedigree of family ID01 from Iran. Black symbol denotes the individual affected with the disorder while open symbols represent the unaffected individuals. Strikethrough denotes deceased individuals. Genotypes for the *TMEM251* (NM_001098621.1) variant c.215dupA; p.(Tyr72Ter) of all participants are shown under the respective symbols. Asterisks mark the individuals whose samples were subjected to exome sequencing. (c) Individuals III:11 and III:9 at the ages of 9 and 13, respectively. Photographs show progressive coarsening of facial features, short stature, and skeletal deformities. The younger child does not have facial dysmorphism but the older brother has mild coarsening of features, short stature, and prominent wrists. (d) The protruding abdomen of individual III:9. (e) Bedridden individual III:5, who is now deceased, at the age of 22 years. Note the coarse facial features with a broad nose and prominent lips. Arms and hands are short, wrist joints are prominent. (f) Photographs of the affected child from Iranian family ID01. Coarse facial features and deformity are evident

(MIM# 607838), *IDUA* (MIM# 611542), and *ARSB* (MIM# 611542). Samples from two affected individuals III:5 and III:9 from family NMD02 were chosen for exome sequencing using the Agilent human V5 kit (51 Mb; Agilent Technologies). Paired-end reads were obtained at 50× average target coverage on an Illumina Hi-Seq 2500 sequencer (Otogenetics). Samples from parents and the affected child were assessed by exome sequencing for family ID01.

For family NMD02, we analyzed the exome data for identification of variants unique to each patient, as well as for those identical to both affected individuals. Variants in the known genes for mucolipidosis and mucopolysaccharidosis (Table S1) were also checked. All homozygous variants and compound heterozygous variants in the exome data were examined further after filtering. Variants with allele frequencies of <0.01 in all public databases were retained. A further choice was made for exonic missense, nonsense frameshift, and in-frame insertion or deletion variants. Synonymous and intronic variants affecting splice sites or creating new splice sites were also considered.

Exome variant call files for two affected individuals of NMD02 were analyzed with AgileVariantMapper as described (Carr et al., 2013) to display regions of homozygosity in individual data, and those common to both samples were identified (Figure S1). Exome coverage data were examined to identify incompletely sequenced exons in one or both of the samples. Those exons located within regions of shared homozygosity were Sanger sequenced after amplification with specific primers (Table S2) using a standard polymerase chain reaction (PCR) protocol or a protocol for GC-rich amplification (Naz & Fatima, 2013).

Data for the three samples of family ID01 was analyzed by Burrow Wheel Aligner (Li & Durbin, 2009), GATK (McKenna et al., 2010), and ANNOVAR (Wang et al., 2010).

2.4 | Computational analyses and databases accessed

We utilized wAnnovar for analyzing the exome data to prioritize variants. The output file of this analysis included the frequency of each variant in large public databases as well as predictions of pathogenicity of missense variants by multiple software. Pathogenicity scores for all missense variants according to REVEL were examined by downloading individual chromosomal files. The computational tools PredictProtein and ProtFun 2.2, were used to predict the secondary structure, identify motifs, and suggest possible protein function. Multiple sequence alignments of the protein sequences were performed with Clustal Omega using vertebrate orthologous sequences obtained by accessing NCBI. Conserved domains of protein were detected through the NCBI search. Predicted or known RNA expression and protein localization were accessed through dbEST, ProteinAtlas, GeneCards, and UniProt. Genomic sequences were downloaded from or visualized at UCSC genome browser hg 19. No parameters were required to be set or changed for using any of these programs or databases.

2.5 | Complementary DNA (cDNA) synthesis

We extracted RNA from the blood (human) or brain, liver, and kidney (mouse) using Tri Reagent (Thermo Fisher Scientific). The cDNA libraries were prepared using RevertAid First Strand cDNA Synthesis Kit (Thermo Fisher Scientific) primed with a Poly T primer. *TMEM251* cDNA was amplified using gene-specific primers (Table S3). The cDNA was cloned by T/A cloning into the pTZ57R/T vector (Thermo Fisher Scientific) and sequence verified.

2.6 | TMEM251 green fluorescent protein (GFP) fusion constructs

The plasmid pACGFP-N1 (Clontech, Takara Bio) was used for obtaining GFP fusion at the C-terminal of TMEM251. *TMEM251* cDNA cloned in pTZ57R/T vector was amplified using gene-specific primers with flanking recognition sequences for restriction enzymes *BamH1* and *EcoR1* (Table S4). Ligation of restriction digested PCR amplified *TMEM251* cDNA and similarly cut vector was completed using T4 DNA ligase. The recombinant plasmid was transformed into competent *Escherichia coli*. The bacteria were plated on LB agar containing 100 μg/ml of kanamycin and grown at 37°C overnight. Colonies were picked and plasmids were isolated using a Qiagen Minikit (Qiagen). Insertion of cDNA into vector was confirmed by sequencing. Site-directed Ligase Independent Mutagenesis was carried out to introduce the c.133C>T;p.(Arg45Trp) variant into the wild-type *TMEM251* cDNA cloned in pACGFP-N1 as described (Chiu et al., 2004). Briefly, an inverse PCR was done in two reactions to amplify the template plasmid containing the cloned wild-type *TMEM251* open reading frame using two-tailed long and two short primers (Table S4).

2.7 | Transfections, immunocytochemistry, and confocal microscopy

Human osteosarcoma cells (Sigma-Aldrich) were grown in DMEM (Sigma-Aldrich) complete medium to a confluency of 70% and then C-terminal GFP fused wild-type or mutant TMEM251 was transiently transfected using Lipofectamine 3000 (Thermo Fisher Scientific) following the manufacturer's protocol. Cells were fixed in 4% paraformaldehyde and blocked using 5% anti-goat serum in 0.1% triton X100/phosphate-buffered saline (PBS). The primary antibodies protein disulfide isomerase (PDI) mouse monoclonal antibody (Enzo Life Sciences) for endoplasmic reticulum and giantin mouse monoclonal antibody for the Golgi complex (Enzo Life Sciences) were diluted in blocking medium to a final dilution of 1 in 100. Secondary staining was completed by using Goat anti-Mouse IgG Cross-Adsorbed Secondary Antibody (Thermo Fisher Scientific) diluted in blocking medium to a final dilution of 1 in 2000. Coverslips were mounted onto slides using Vectashield® hardset mounting media containing DAPI (Vector Laboratories). Intracellular localization of both the wild-type and the mutant TMEM251 GFP fusions (GFP fused at C-terminal)

were observed by confocal imaging of the transfected cells after immunostaining. Human osteosarcoma cells were examined with an LSM 700 Laser Scanning Microscope (Carl Zeiss) equipped with Zeiss AxioCam camera (Carl Zeiss) and ZEN 2011 digital imaging software (Carl Zeiss).

2.8 | Chondrocyte isolation and culture

Proximal tibia and distal femur growth plates were dissected from 3 to 5-day old rats (Charles River Laboratory) and digested with 0.3% collagenase type IA (Sigma-Aldrich) in DMEM/F12 aseptically, as previously described (Spath et al., 2018). Briefly, dissected cartilage pieces were washed twice in PBS with 1% penicillin/streptomycin, 50 ng/ml fungizone (both from Thermo Fisher Scientific), next incubated with 0.1% EDTA (Sigma-Aldrich) in PBS for 15 min and 0.125% trypsin (Thermo Fisher Scientific) in PBS for 30 min, all steps at 37°C while shaking. Cartilage pieces were washed twice in PBS with 1% penicillin/streptomycin, 50 ng/ml fungizone, and digested at 37°C while shaking with 0.3% collagenase type IA (Sigma-Aldrich) in DMEM/F12 by repeating cycles of 30 min until digestion was complete. The cell suspension was filtered through a 70 μm-cell strainer (BD Biosciences), spun at 300 g for 5 min, washed twice in PBS containing 1% penicillin/streptomycin, 50 ng/ml fungizone (Thermo Fisher Scientific). The isolated chondrocytes were resuspended and cultured at 37°C, 5% CO_2 in DMEM/F12 with GlutaMAX (Thermo Fisher Scientific) supplemented with 10% fetal bovine serum (FBS), 50 μg/ml ascorbic acid (Thermo Fisher Scientific), 1% penicillin/streptomycin and 50 ng/ml fungizone.

2.9 | Small interfering RNA (siRNA) knockdown of *Tmem251*

Two sets of predesigned *Silencer Select* siRNA against rat *Tmem251* (s179664: GACAGUUAUUUUCUUGAUAtt, and s179666: GGAUUGGAGUGGGAUUGUAtt) were obtained from Life Technologies® (Thermo Fisher Scientific). siRNA against *Gapdh* (4390849) was used as a positive control and scrambled siRNA (4390843) was used as a negative control.

2.10 | Chondrocyte transfection with siRNAs

Chondrocytes (25,000/cm^2) were cultured in 24-well plates and transfected with *Tmem251* specific or control siRNA when 60% confluency was reached, as described (Lui et al., 2016). Briefly, cells were washed 1 h before transfection with PBS, and the medium was changed to DMEM/F12 without any antibiotics. Chondrocytes were separately transfected with 40 nM of negative control siRNA, two siRNAs against *TMEM251* (s179664 or s179666), and *Gapdh* siRNA (Thermo Fisher Scientific) using Lipofectamine 3000 (Thermo Fisher Scientific) according to manufacturer's instructions. Sixteen hours post-transfection, the chondrocyte culture medium was replaced back to DMEM/F12 with GlutaMAX supplemented with 10% FBS, 50 μg/ml ascorbic acid, 1% penicillin/streptomycin, and 50 ng/ml fungizone.

2.11 | Quantitation of gene expression by real-time PCR

Cell lysates were collected 48 h posttransfection in solution C (4 M guanidine thiocyanate, 25 mM sodium citrate pH 7, 0.1 M β-mercaptoethanol). Total RNA was extracted using phenol, chloroform as previously described (Spath et al., 2018). Total RNA (50 ng) was reverse-transcribed into cDNA by Superscript Reverse Transcriptase III (Thermo Fisher Scientific). Expression of *Tmem251*, *Alpl*, and *Col2a1* was quantified by ABI Prism 7900 Fast Sequence Detector (Thermo Fisher Scientific) by using specific primers (Table S5) and SYBR green (Thermo Fisher Scientific). Data were normalized to 18S ribosomal RNA and relative expression was calculated by using the formula: $2^{-\Delta C_t} \times 10^6$, with ΔC_t being target gene expression relative to 18S ribosomal RNA (Nilsson et al., 2007).

2.12 | Statistical analyses

The logarithm of odds (LOD) scores for data of NMD02 was calculated using the MLINK program of the Linkage 3.3 package (Terwilliger & Ott, 1994). Only the participating branch was included for the purpose of LOD score calculations.

The siRNA experiments were independently performed twice, and for each experiment, we had triplicates for each condition. The values in the graphs were calculated and presented as the average ± *SE* of the mean of technical replicates. Significance of each siRNA-treated sample compared to scrambled control was calculated by unpaired *T* test, using GraphPad Prism 7.0 (GraphPad Software, Inc.) using raw data for absorbance and qPCR.

2.13 | Proliferation and apoptotic cell death assessment

Proliferation, apoptosis, and RNA expression were investigated 48 h posttransfection. Proliferation was assessed by colorimetric detection based on 5-bromo-2′-deoxyuridine (BrdU) incorporation (Roche), according to the manufacturer's protocol. Briefly, cells were incubated with BrdU for 3 h, and absorbance was read at 370 nm (SpectraMax Plus 384 Microplate Reader, Molecular Devices LLC) 48 h posttransfection. Cells incubated for few seconds with BrdU were used as background control.

Apoptosis was measured 48 h posttransfection by photometric detection of cytoplasmic histone-associated DNA fragments in cell lysates according to the manufacturer's instructions (Roche). Briefly, cell lysates were loaded onto a streptavidin-coated plate and

subsequently incubated with biotinylated anti-histone antibodies and anti-DNA antibodies conjugated with peroxidase (POD). Unbound antibodies were removed by washing. Substrate solution, tetramethyl-benzidine (Roche), was added. The POD activity in the immunocomplex was determined photometrically at 405 nm.

3 | RESULTS

3.1 | Clinical features

Family NMD02 (Figure 1a) had seven individuals while family ID01 had one child (Figure 1b) affected with symptoms resembling a mucolipidosis II α/β like syndrome (MIM# 252500) (Table 1). Five affected individuals in family NMD02 were siblings and alive when the study was initiated. Two (III:5, III:6) of these affected individuals died during the course of the study. The parents and six siblings of the five patients were healthy with no obvious phenotype. The affected siblings had similar phenotypes (Figure 1c,d,e). However, the phenotype of the youngest affected individual was less severe as compared to that manifested by the older siblings, supporting a progressive course of the disorder (Table 1). Coarsening of facial features was more severe in the oldest siblings. Two affected individuals (III:5 and III:6) lost walking ability due to the increasing severity of joint contractures and became bedridden in the late teens. They both died in their early twenties. Cognition of all affected individuals was average and the patients responded to questions and their speech was not impaired. Complete blood counts of individuals III:9 and III:11 detected mild anemia but no other abnormality (Table 1). Clinical or imaging investigations apart from skeletal radiography were not possible due to limited access to proper health care.

TABLE 1 Phenotypic details of affected individuals of families NMD02 and ID01

	NMD02					ID01
ID	III:5	III:6	III:9	III:10	III:11	IV:5
Sex	F	F	M	F	M	F
Age of onset (years)	1	1	1	1	1	6 months
Age in 2013 (years)	24	20	13	11	9	NA
Age in 2017 (years)	NA[a]	NA[b]	17	15	13	3[c]
Height in 2013 (cm)	82.2	79.2	82.2	79.2	82.2	NA
Height in 2017 (cm)	NA[a]	NA[b]	91.4	87.6	91.4	NA
Height *SD* score	−11.1	−11.6	−11.9	−8.8	−8.5	NA
Walking ability	Progressively lost and bed ridden	+	+	Impaired at age of 14	+	-
Cognition	Normal	Normal	Normal	Normal	Normal	NA
Speech	+	+	+	+	+	2-3 words
Distended abdomen	+	+	+	+	+	-
Scoliosis	NA	NA	+	NA	+	+
Complete blood count[d]	NA	NA	+	NA	+	+
GAG in urine[e]	NA	NA	-	-	-	NA
Lysosomal enzymes from dried blood						
Iduronate-2 sulfatase activity	NA	NA	NA	NA	NA	4109 pmol/spot × 20 h (Ref: 200–2614 pmol/spot × 20 h)
α-Iduronidase activity	NA	NA	NA	NA	NA	17,008 pmol/spot × 20 h (Ref: 400–3300 pmol/spot × 20 h)
β-Galactosidase activity	NA	NA	NA	NA	NA	0.47 pmol/spot × 20 h (Ref: 0.5–3.2 pmol/spot × 20 h)
Radiographs	NA	NA	Dysostosis multiplex	NA	Dysostosis multiplex	Dysostosis multiplex

Note: β-Galactosidase activity is almost within the normal range.
Abbreviations: +, present; −, absent; GAG, glycosaminoglycans; NA, not applicable or not assessed.
[a]Deceased at the age of 24 years.
[b]Deceased at the age of 21 years.
[c]Deceased at the age of 5 years.
[d]Test obtained in 2017.
[e]Detected by Berry spot test.

Family ID01 was identified in Iran with one affected girl with the onset of symptoms at the age of 6 months (Figure 1f). She had severe skeletal dysplasia, coarse facial features, developmental delay, short stature, craniosynostosis, kyphoscoliosis, hip joint subluxation, abnormal teeth, upper airway problem, and motor impairment. Brain MRI showed thinning of the corpus callosum and mild ventriculomegaly. Heart echocardiography documented a small ventricular septal defect. Biochemical tests for metabolic disorders showed an increase in Iduronate-2 sulfatase (Table 1).

Radiographs of individuals III:11 and III:9 (Figure 2a,b) in family NMD02 indicated severe skeletal dysplasia, some features of dysostosis multiplex with additional abnormalities suggesting a previously uncharacterized skeletal dysplasia. The long bones were severely affected by prominent metaphyseal regions and abnormal epiphyses. Pelvic radiograph of individual III:11 revealed small iliac wings, hypoplastic acetabular roof, and abnormal proximal hips with long femoral necks. The skeletal anomalies were more severe in the older sibling, supporting the progressive nature of the disorder.

Radiographs of the affected child from family ID01 indicated severe skeletal dysplasia. Multiple hemivertebrae, paddle shape ribs, hypoplasia, and flattening of the acetabular roof were also revealed by radiography (Figure 2c). Diaphyseal widening in humerus with hypoplastic epiphysis and hypoplastic glenoid fossa was evident. Moreover, hip radiographs indicated short iliac wings and left hip dislocation. The child died at the age of 5 years due to respiratory failure.

3.2 | Genetic analyses

Fluorescently labeled microsatellite markers located close to the respective genes (Table S1) excluded linkage of the disorder to *GNPTAB* (MIM# 607840), *GNPTG* (MIM# 607838), *IDUA* (MIM# 611542), and *ARSB* (MIM# 611542) for family NMD02. Analyses of the filtered exome data revealed three rare homozygous exonic variants located on chromosome 14q32 (Table S6) which also segregated with the phenotype in family NMD02 (Figures 1 and 2). Only *TMEM251* NM_001098621.1 variant c.133C>T;p.(Arg45Trp), was predicted to be damaging by all five prediction programs and affected an amino acid that was fully conserved in the orthologous proteins (Figure 3a). This variant was absent from all public databases and was not detected in 400 ethnically matched control chromosomes. The known genetic causes of various forms of mucopolysaccharidoses and mucolipidosis were also excluded by analyses of exome data for family NMD02 (Table S1).

We identified five regions of shared homozygosity located on different chromosomes from the exome data of the two affected individuals (Figure S1). Sanger sequencing of the variants located in these regions revealed that only variants present on chromosome 14q32 (Tables S2 and S6 and data not shown) segregated with the phenotype with a LOD score of 3.2 at $\theta = 0$. Moreover, no variants were identified by Sanger sequencing in those exons, which were located within the chromosome 14q32 region of shared homozygosity (Figure S1) and had not been covered by exome sequencing (Table S2).

Analysis of the trio exome sequencing data of family ID01 revealed one homozygous insertion variant c.215dupA;p.(Tyr72Ter) in *TMEM251* in the patient, for which the parents were heterozygous carriers (Figures 1 and 2). None of the other 23 individuals from the pedigree were found to be homozygous for the variant. Moreover, this variant was absent from all public databases. The variant identified in family NMD02 was deposited in LOVD (#0000601066) and the variant identified in family ID01 was deposited in ClinVar (SCV000998897).

3.3 | *TMEM251* and *TMEM251P*

TMEM251, also known as *C14orf109* is an uncharacterized gene located on chromosome 14q32.12. *TMEM251* is a highly conserved gene (0.69 Z score and 21.351GDI score) and the identity among orthologues and the presence of very few variants in controls points to the evolutionary importance of the protein. The two isoforms, NM_001098621.1 and NM_015676.1 of the gene are encoded by alternatively spliced exons in mammals while the genomes of other vertebrates have sequences corresponding to only one of the shorter isoforms (Figure 3b). A processed pseudogene of *TMEM251* long isoform, *TMEM251P*, which contains multiple stop codons in the corresponding reading frame, is located on the reverse strand within intron 85 of *ADGRV1* on chromosome 5:90326406-90327386 (hg19) (Figure 3c). The pseudogene is present in one to two copies in all primate genomes examined and is absent from the genomes of other vertebrates.

3.4 | *TMEM251* expression and protein domains

Analyses of human expressed sequence tag (EST) data suggested that both the long isoform and the short isoform are expressed in various tissues, with the short isoform preferentially expressed in the brain as compared to the long isoform. We obtained transcripts for both isoforms of *TMEM251* from blood, which was the only source of human RNA available to us. We were able to amplify *Tmem251* from cDNA libraries mouse tissues including heart, brain, liver, and kidney. In zebrafish, higher expression of *tmem251* mRNA is detected in the axis at early somitogenesis as compared to other regions starting from one cell to the pectoral fin stage (Thisse & Thisse, 2014). *Tmem251* is also expressed in ovine muscles and is upregulated in skeletal muscles of callipyge lambs (Vuocolo et al., 2007).

TMEM251 has a conserved domain of unknown function (DUF4583) corresponding to amino acids 40 to 167 (NP_001092091.1) in the 169 amino acid protein in the human long isoform (Figure 3b). The short isoform lacks 35 amino acids from the N-terminal (Figure 3b). TMEM251 is predicted to be a transmembrane protein with two α helices (Figure 3d). No signal peptide was detected in the protein sequence by computational analyses. The N- and C-terminal are

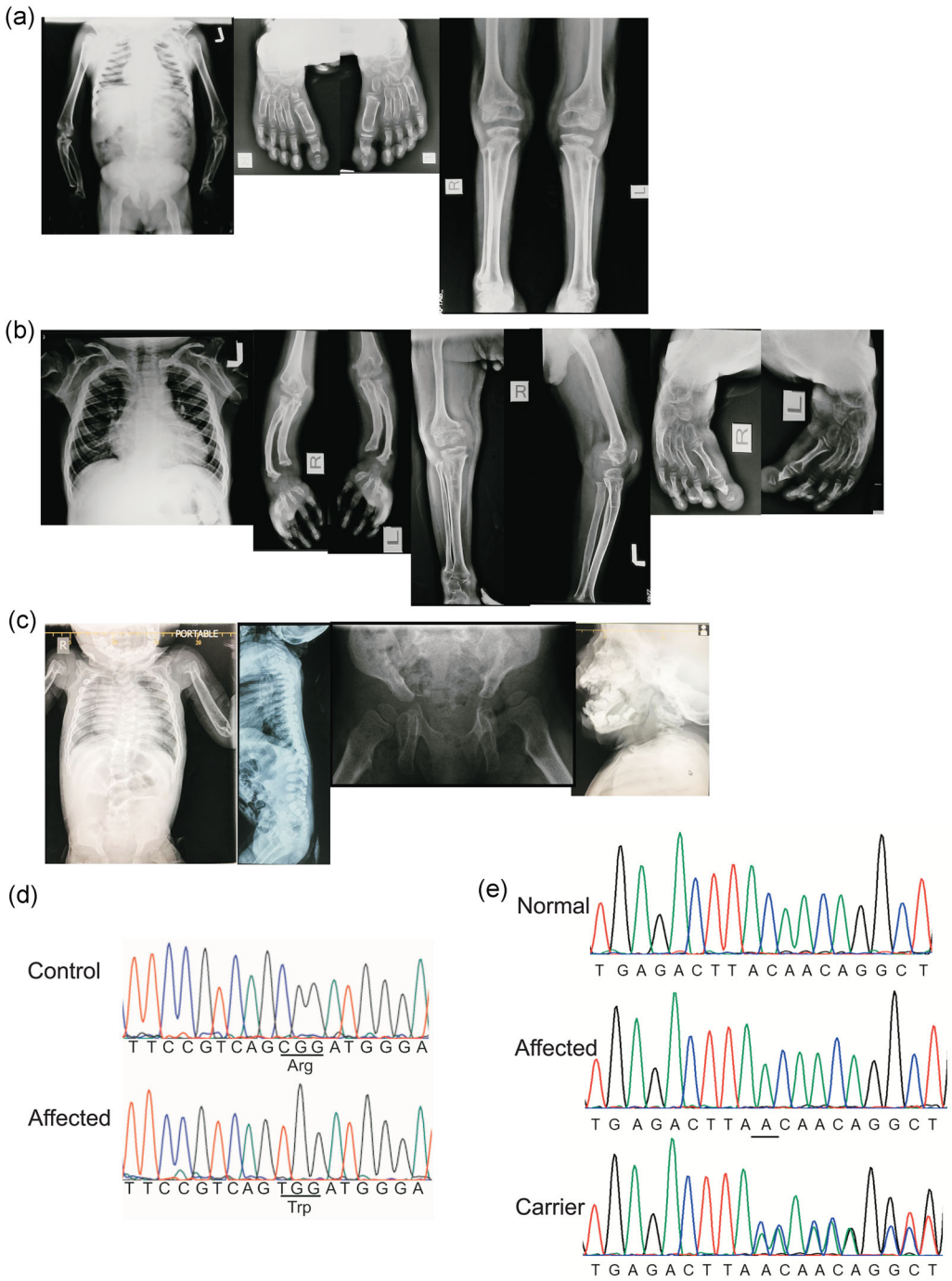

FIGURE 2 Radiographic and genetic findings in families NMD02 and ID01. (a) Radiographs of individual III:11 of NMD02 show widened ribs with a normal shaped thorax. Thoracic vertebrae are of reduced height. Iliac wings are abnormal and acetabular roof is hypoplastic. Femur, tibia, and fibula are irregularly shaped with elongated femoral necks and abnormal epiphyses. Feet show poor mineralization, curving of the metatarsal bones with osteolytic appearance of the joints. Epiphyses are irregular and abnormal in shape. Distal parts of the first toe have an osteolytic appearance on both sides. (b) Radiographs of individual III:9 of NMD02. Thoracic and lower limb radiographs indicate similar but more severe features as in individual III:11. Forearms are clearly abnormal with curved and abnormally shaped radius and ulna with distal osteolysis. (c) Radiographs of an affected child from the Iranian family. Spine radiograph indicates scoliosis due to multiple hemivertebrae and paddle shape ribs. Pelvic radiograph shows hypoplasia and flattening of the acetabular roof and bilateral hip dislocation with short iliac wings. (d) Variant trace of *TMEM251* (NM_001098621.1) c.133C>T; p.(Arg45Trp) at site of variation. The changed base is shown by an arrow, while the affected codon is underlined. (e) Variant trace of *TMEM251* (NM_001098621.1) c.215dupA; p.(Tyr72Ter) at the site of variation. The inserted base is shown by an arrow, while the affected codon is underlined

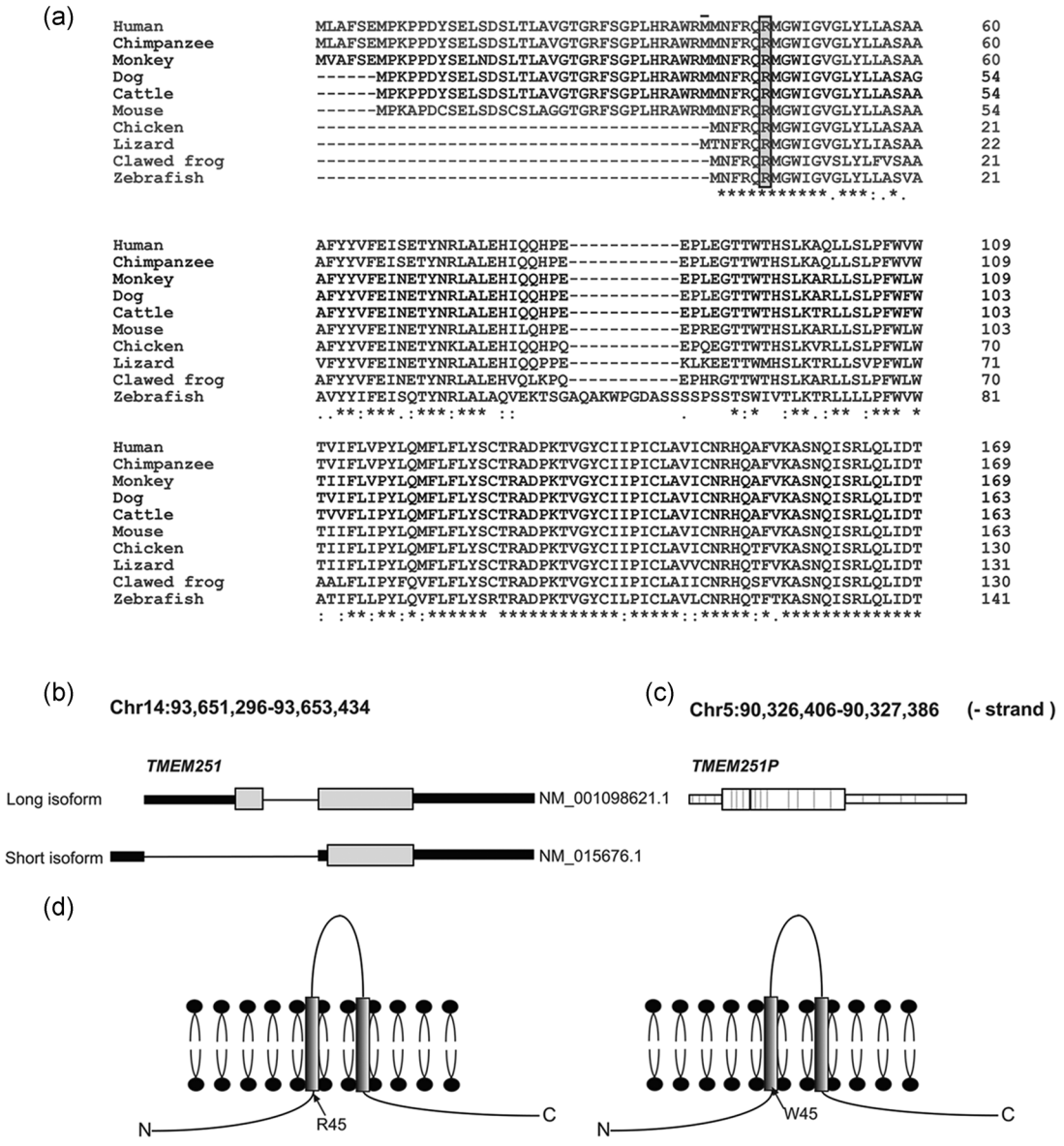

FIGURE 3 Multiple sequence alignment and graphical representation of TMEM251. (a) CLUSTAL Omega multiple sequence alignment of TMEM251 (NP_001092091.1) with orthologues from diverse vertebrate species. The gaps in alignment are denoted by dashes. Identical amino acids in all orthologues are indicated by asterisks below the alignment. The colons and periods depict amino acids that are highly conserved or less conserved, respectively. The p.Arg45 residue affected by the variant is boxed. The first amino acid of the short isoform of TMEM251 is depicted by a small horizontal bar on top of the methionine residue (NP_056491.1, XP_003832843.1, NP_001180781.1, XP_003435108.1, XP_010815578.1, NP_796114.1, NP_796114.1, NP_796114.1, NP_796114.1, and NP_796114.1). (b) Schematic representation of human *TMEM251*. Both the long (NM_001098621.1) and short isoforms (NM_015676.1) are depicted. Gray boxes show the coding exons while the untranslated regions are indicated by black bars. An intron is represented by a horizontal line. The short isoform of the gene encodes a protein that lacks 38 amino acids from the N-terminal which are present in the long isoform. (c) Illustration of the processed pseudogene of *TMEM251* long isoform which is located on chromosome 5 (90,326,406–90,327,386) within intron 85 of *ADGRV1* (− or antisense strand). The gray vertical lines denote mismatches to the *TMEM251* sequence. (d) Diagrammatic representation of TMEM251 (NP_001092091.1 and NP_056491.1) as encoded by the long isoform, inserted in the lipid bilayer of the plasma membrane. The two transmembrane regions are shown by shaded rectangles (amino acids 47–66 and 105–127, respectively). N and C denote the amino and carboxyl-terminal of the protein, respectively. The positions of the wild-type protein with p.Arg45 (left panel) and the variant p. Trp45 (right panel) are depicted by arrows. Note that the variant is predicted to result in inclusion of amino acid 45 into the first transmembrane segment which will be inserted in the membrane (right panel)

predicted to face the lumen. ProtFun 2.2 analyses predicted TMEM251 to be a transporter with high odds of 4.139.

The missense variant p.(Arg45Trp) (NP_001092091.1), or p.(Arg7Trp) (NP_056491.1) affects an amino acid located close to the first transmembrane segment at the amino-terminal of both isoforms of the protein. The variant is predicted to result in the incorporation of the mutated amino acid tryptophan inside the membrane as part of the first transmembrane segment making it unavailable in the

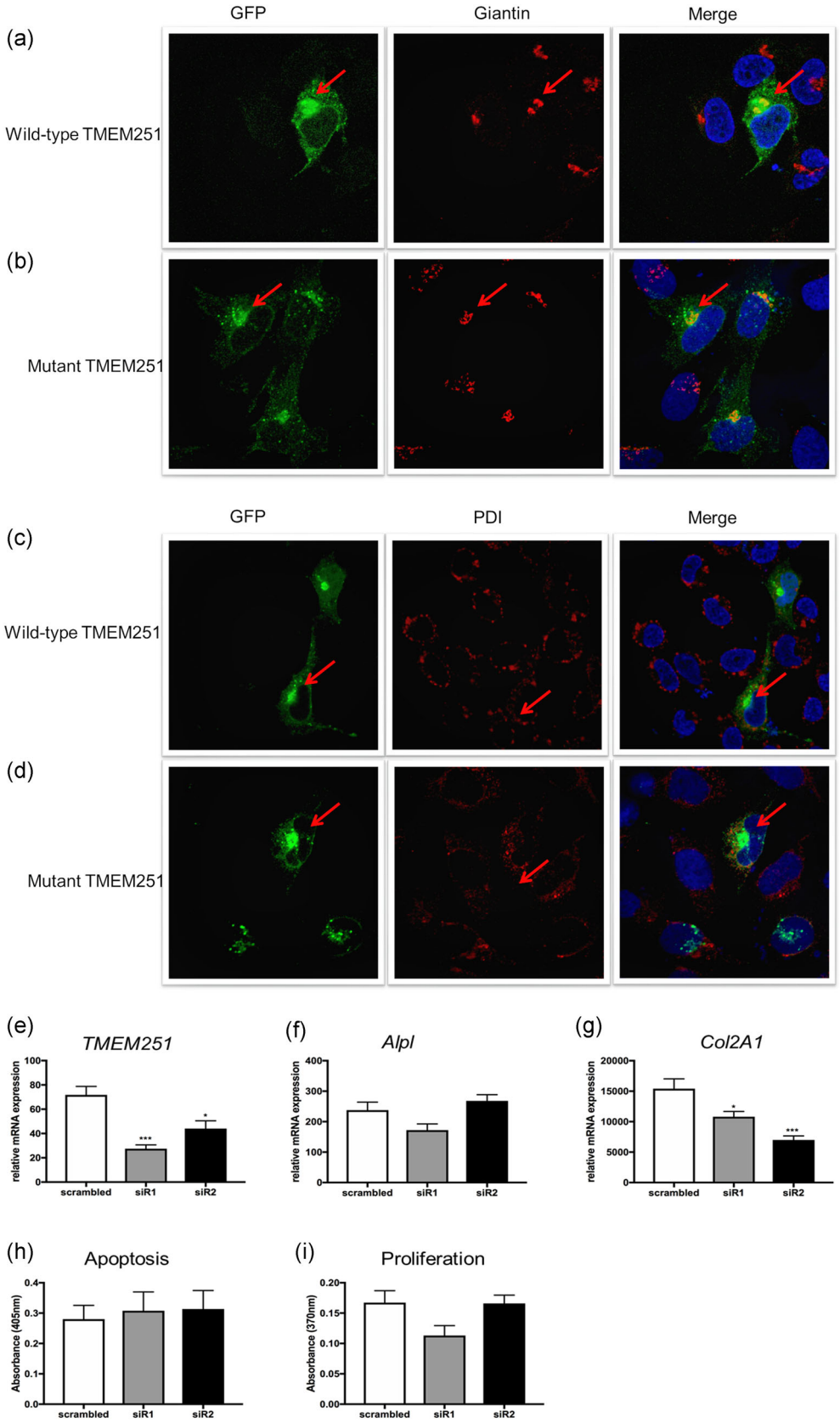

lumen (Figure 3d). This effect is similar to that predicted for an arginine to tryptophan variant pathogenic allele of TMEM230 in Parkinson's disease (Deng et al., 2016). The frameshift variant c.215dupA;p.(Tyr72Ter) is predicted to truncate the protein in the nontransmembrane segment located between the two transmembrane regions which may give rise to a shortened protein that could be unstable. No protein may be produced at all if nonsense-mediated decay of the mutant transcript occurs.

3.5 | TMEM251 localizes to the Golgi complex

Online searches indicated that TMEM251 is likely to be localized to the Golgi complex and the plasma membrane in humans and mice. GFP-fused wild-type TMEM251 was observed to strongly colocalize with a marker of Golgi complex, giantin, in transiently transfected human osteosarcoma cells (Figure 4a). GFP-fused p.Arg45Trp TMEM251 also localized to the Golgi complex (Figure 4b). In contrast, both the wild-type and mutant proteins did not colocalize with the markers of the endoplasmic reticulum (PDI) (Figure 4c,d) or lysosome (LAMP1) (not shown). The localization of GFP-fused p.Arg45Trp TMEM251 was markedly reduced and punctate when compared to that of the wild-type protein (Figure 4b,d). However, measurements were not performed to quantify these differences.

3.6 | *Tmem251* knockdown induces chondrocyte dedifferentiation

Two different siRNAs decreased *TMEM251* expression by 2.6-fold ($p < .001$) and 1.6-fold ($p < .01$), respectively, 48 h after transfection of rat primary chondrocytes, compared to chondrocytes transfected with scrambled siRNA (Figure 4e). To determine whether *Tmem251* knockdown affects chondrocyte differentiation, we investigated the expression levels of chondrocyte differentiation markers, such as alkaline phosphatase (*Alpl*) and collagen type 2 (*Col2a1*). Expression of chondrogenic markers was not altered in cells treated with scrambled siRNA. In contrast, *Tmem251* knockdown did not affect *Alpl* expression (Figure 4f) but significantly reduced *Col2a1* expression by 1.4-fold ($p < .05$) and 2.2-fold ($p < .001$), respectively, for the two siRNAs tested (Figure 4g). Reduction of *Col2a1* expression, but not *Alpl* expression in *Tmem251* knockdown cells, suggests that TMEM251 is important for chondrocytic, but not hypertrophic differentiation, and is perhaps particularly required for maintenance of the chondrocytic phenotype (Ma et al., 2013).

3.7 | *Tmem251* knockdown does not affect apoptosis or chondrocyte proliferation

Tmem251 knockdown did not affect chondrocyte apoptosis 48hrs posttransfection (Figure 4h), indicating that increased apoptosis of chondrocytes may not be a major pathogenic mechanism in this condition. Moreover, chondrocyte proliferation was not significantly affected by *Tmem251* knockdown (Figure 4i). In summary, the *Tmem251* knockdown experiment demonstrated that TMEM251 is important for chondrocytic differentiation.

4 | DISCUSSION

We have identified two novel homozygous variants in *TMEM251* as the likely cause of a complex progressive skeletal disorder leading to severe short stature and early mortality in two unrelated families. Our findings suggest that *TMEM251* may have a metabolic role. This is specifically supported by the abnormal activities of three lysosomal enzymes detected from the sample of the patient from family ID01 (Table 1). Elevated lysosomal enzyme activity has also been previously reported for patients with mucolipidosis (Singh et al., 2017). Moreover, the clinical course of disease in both families was

FIGURE 4 Localization of wild-type and mutant TMEM251 proteins in human osteosarcoma cell line and knockdown of *Tmem251* in rat primary chondrocytes. (a) Analysis of wild-type TMEM251 localization in cells transfected with GFP-fused TMEM251 and immunostaining of Golgi complex with antibody against giantin (red) nuclei with DAPI (blue). Merged image (yellow) indicates colocalization of wild-type TMEM251 with Golgi marker. (b) Analysis of mutant TMEM251 localization in cells transfected with GFP-fused mutant TMEM251 and immunostaining of Golgi complex with antibody against giantin (red) nuclei with DAPI (blue), merged image (yellow) indicates colocalization of mutant TMEM251 with Golgi marker. (c) Immunostaining of ER with anti-PDI antibody after transfection with wild-type TMEM251 merged image indicates separate localization of wild-type TMEM251 and ER marker. (d) Immunostaining of Endoplasmic Reticulum with anti-PDI antibody after transfection with mutant TMEM251, merged image demonstrate mutant TMEM251 does not localize to ER. Note the reduced and punctate expression of mutant TMEM251 as compared to wild-type TEM251 (images were taken in green, red, and blue channel, separately and then merged). (e) Transfection of rat chondrocytes with two siRNAs (siR1 and siR2) against *Tmem251* reduced mRNA expression of *Tmem251*, as determined by quantitative PCR. (f) *Alpl* expression measured by quantitative PCR in transfected cells (see (g)). (g) *Col2a1* expression measured by quantitative PCR in transfected cells compared to scrambled control. *Alpl* expression was not significantly changed in siR2 transfected cells, whereas *Col2a1* expression was reduced in cells transfected with either siR1 or siR2. (h) Apoptosis in rat chondrocytes is not altered by *Tmem251* knock-down, as measured by detection of cytoplasmic histone-associated-DNA-fragments. (i) Proliferation of chondrocytes measured by BrdU incorporation indicates no effect on proliferation upon *Tmem251* knockdown. All measurements were performed 48 h posttransfection. Bars indicate average ± SEM of two independent experiments (*$p < .05$; ***$p < .001$ relative to the scrambled-siRNA treated cells). BrdU, 5-bromo-2′-deoxyuridine; DAPI, 4′,6-diamidino-2-phenylindole; ER, endoplasmic reticulum; GFP, green fluorescent protein; PCR, polymerase chain reaction; PDI, protein disulfide isomerase; siRNA, small interfering RNA

suggestive of a metabolic multisystemic disorder which was further supported by the widespread *TMEM251* expression pattern.

The affected individuals in the two families had striking phenotypic similarities to patients with mucolipidosis and mucopolysaccharidosis (Mortier et al., 2019), specifically to mucolipidosis II/III based on patient characteristics of short stature, severe progressive skeletal dysplasia, severe physical handicap, facial dysmorphology, and distended abdomens (Dr. JG Leroy, personal communication). However, variants in the causative genes for these disorders (*GNPTAB* or *GNPTG)* were excluded as the cause of the phenotype. Interestingly, both GNPTAB and GNPTG localize to the Golgi complex, as is the case for TMEM251. Studies are required to test whether the three proteins participate in the same cellular pathways.

The unavailability of patients' cells for RNA or protein expression studies hinders the evaluation of the variants' effects in vivo. Cardiac and brain imaging studies in the Iranian patient suggested the pathogenic variants in this gene could be responsible for cardiac and brain abnormalities as well. The unavailability of abdominal and cardiac imaging and laboratory examinations for the Pakistani family, however, precluded further investigations to unravel organ abnormalities, including hepatosplenomegaly and cardiac anomalies. We were also not able to perform more extensive metabolic investigations and the potential metabolic role of TMEM251 needs to be further clarified.

Our results indicate that the p.(Arg45Trp) variant could be a functional null allele while the p.(Tyr72Ter) may also be a loss of function allele. The decreased localization of p.(Arg45Trp) TMEM251 to the Golgi complex could be due to improper folding of the protein. This may halt its incorporation into the membranes or cause degradation of the mutant TMEM251. The reduction in chondrogenic marker *Col2a1* after siRNA-induced knockdown of *Tmem251* in rat primary chondrocytes suggests that TMEM251 may play a role in the differentiation of chondrocytes and thus have an important function in the development of cartilage and bones. Future studies of animal models with *Tmem251* variants could elucidate the role of the encoded protein in skeletogenesis in more detail.

In conclusion, our findings implicate homozygous *TMEM251* variants as the genetic cause of a severe novel skeletal dysplasia with features of a metabolic disorder. Identification of additional affected individuals due to *TMEM251* variants will delineate the full spectrum of the disorder and expand phenotypic manifestations as well as the molecular mechanisms involved in the disease course. Continued research will elucidate the role of TMEM251 in human physiology.

ACKNOWLEDGEMENTS

We are highly grateful to the members of families NMD02 and ID01 for their participation and co-operation in the study. We thank Dr. JG Leroy for helpful comments. One author (NA) was a recipient of an indigenous and an IRSIP scholarship from the Higher Education Commission, Pakistan. This study was supported by personal funds (NM), NIMAD research grant (940714) award (MAF), Swedish Research Council (OM), Academy of Finland (OM), Sigrid Jusélius Foundation (OM), and a grant from Koshish Foundation, USA (SN).

CONFLICT OF INTEREST

The authors declare they have no conflict of interest.

WEB RESOURCES

AgileVariantMapper: http://www.insilicase.com/agile/AgileVariantMapper.aspx

Clustal omega, ClutalO: https://www.ebi.ac.uk/Tools/msa/clustalo/

GeneCards: https://www.genecards.org/

NCBI Conserved domains search: https://www.ncbi.nlm.nih.gov/Structure/cdd/wrpsb.cgi

NCBI Nucleotide sequence search: https://www.ncbi.nlm.nih.gov/

ProteinAtlas: http://www.proteinatlas.org/search/tmem251

ProtFun 2.2: http://www.cbs.dtu.dk/services/ProtFun/

Rare Exome Variant Ensemble Learner, REVEL: https://sites.google.com/site/revelgenomics/

UCSC genome browser: https://genome.ucsc.edu/

UniProt: https://ebi16.uniprot.org/

wAnnovar: http://wannovar.wglab.org/

DATA AVAILABILITY STATEMENT

Data is available from corresponding authors upon reasonable request.

ORCID

Outi Makitie https://orcid.org/0000-0002-4547-001X

Sadaf Naz https://orcid.org/0000-0002-1912-0235

REFERENCES

Ballabio, A., & Gieselmann, V. (2009). Lysosomal disorders: From storage to cellular damage. *Biochimica et Biophysica Acta (BBA)-Molecular Cell Research*, *1793*(4), 684–696.

Carr, I. M., Bhaskar, S., O' Sullivan, J., Aldahmesh, M. A., Shamseldin, H. E., Markham, A. F., Bonthron, D. T., Black, G., & Alkuraya, F. S. (2013). Autozygosity mapping with exome sequence data. *Human Mutation*, *34*(1), 50–56. https://doi.org/10.1002/humu.22220

Chiu, J., March, P. E., Lee, R., & Tillett, D. (2004). Site-directed, Ligase-Independent Mutagenesis (SLIM): A single-tube methodology approaching 100% efficiency in 4 h. *Nucleic Acids Research*, *32*(21):e174.

Coman, D., Irving, M., Kannu, P., Jaeken, J., & Savarirayan, R. (2008). The skeletal manifestations of the congenital disorders of glycosylation. *Clinical Genetics*, *73*(6), 507–515.

Deng, H. X., Shi, Y., Yang, Y., Ahmeti, K. B., Miller, N., Huang, C., Cheng, L., Zhai, H., Deng, S., Nuytemans, K., Corbett, N. J., Kim, M. J., Deng, H., Tang, B., Yang, Z., Xu, Y., Chan, P., Huang, B., Gao, X. P., … Siddique, T. (2016). Identification of TMEM230 mutations in familial Parkinson's disease. *Nature Genetics*, *48*(7), 733–739.

Eklund, E. A., & Freeze, H. H. (2006). The congenital disorders of glycosylation: A multifaceted group of syndromes. *NeuroRx*, *3*(2), 254–263.

Krakow, D. (2015). Skeletal dysplasias. *Clinics in Perinatology*, *42*(2), 301–319.

Kranz, C., Basinger, A. A., Güçsavaş-Çalıkoğlu, M., Sun, L., Powell, C. M., Henderson, F. W., Aylsworth, A. S., & Freeze, H. H. (2007). Expanding spectrum of congenital disorder of glycosylation Ig (CDG-Ig): Sibs with a unique skeletal dysplasia, hypogammaglobulinemia, cardiomyopathy,

genital malformations, and early lethality. *American Journal of Medical Genetics, Part A*, *143*(12), 1371–1378.

Li, H., & Durbin, R. (2009). Fast and accurate short read alignment with Burrows–Wheeler transform. *Bioinformatics*, *25*(14), 1754–1760.

Longo, S., Bollani, L., Decembrino, L., Di Comite, A., Angelini, M., & Stronati, M. (2013). Short-term and long-term sequelae in intrauterine growth retardation (IUGR). *The Journal of Maternal-Fetal & Neonatal Medicine*, *26*(3), 222–225.

Lui, J. C., Garrison, P., Nguyen, Q., Ad, M., Keembiyehetty, C., Chen, W., Jee, Y. H., Landman, E., Nilsson, O., Barnes, K. M., & Baron, J. (2016). EZH1 and EZH2 promote skeletal growth by repressing inhibitors of chondrocyte proliferation and hypertrophy. *Nature Communications*, *7*, 13685.

Ma, B., Leijten, J. C. H., Wu, L., Kip, M., van Blitterswijk, C., Post, J. N., & Karperien, M. (2013). Gene expression profiling of dedifferentiated human articular chondrocytes in monolayer culture. *Osteoarthritis and Cartilage*, *21*(4), 599–603.

McKenna, A., Hanna, M., Banks, E., Sivachenko, A., Cibulskis, K., Kernytsky, A., Garimella, K., Altshuler, D., Gabriel, S., Daly, M., & DePristo, M. A. (2010). The Genome Analysis Toolkit: A MapReduce framework for analyzing next-generation DNA sequencing data. *Genome Research*, *20*(9), 1297–1303.

Mortier, G. R., Cohn, D. H., Cormier-Daire, V., Hall, C., Krakow, D., Mundlos, S., Nishimura, G., Robertson, S., Sangiorgi, L., Savarirayan, R., Sillence, D., Superti-Furga, A., Unger, S., & Warman, M. L. (2019). Nosology and classification of genetic skeletal disorders: 2019 revision. *American Journal of Medical Genetics, Part A*, *179*(12), 2393–2419.

Naz, S., & Fatima, A. (2013). Amplification of GC-rich DNA for high-throughput family-based genetic studies. *Molecular Biotechnology*, *53*(3), 345–350. https://doi.org/10.1007/s12033-012-9559-y

Nilsson, O., Parker, E. A., Hegde, A., Chau, M., Barnes, K. M., & Baron, J. (2007). Gradients in bone morphogenetic protein-related gene expression across the growth plate. *Journal of Endocrinology*, *193*(1), 75–84.

Saenger, P., Czernichow, P., Hughes, I., & Reiter, E. O. (2007). Small for gestational age: Short stature and beyond. *Endocrine Reviews*, *28*(2), 219–251. https://doi.org/10.1210/er.2006-0039

Singh, A., Prasad, R., Gupta, A. K., Sharma, A., Alves, S., Coutinho, M. F., Kapoor, S., & Mishra, O. P. (2017). I cell disease (mucolipidosis II alpha/beta): From screening to molecular diagnosis. *The Indian Journal of Pediatrics*, *84*(2), 144–146.

Sparks, S. E., & Krasnewich, D. M. (2017). Congenital disorders of N-linked glycosylation and multiple pathway overview. *GeneReviews[Internet]*®: University of Washington, Seattle.

Spath, S. S., Andrade, A. C., Chau, M., Baroncelli, M., & Nilsson, O. (2018). Evidence that rat chondrocytes can differentiate into perichondrial cells. *JBMR Plus*, *2*(6), 351–361. https://doi.org/10.1002/jbm4.10056

Stanley, P. (2011). Golgi glycosylation. *Cold Spring Harbor Perspectives in Biology*, *3*(4), a005199.

Terwilliger, J. D., & Ott, J. (1994). *Handbook of human genetic linkage*. JHU Press.

Thisse, B., & Thisse, C. (2014). Fast release clones: A high throughput expression analysis. 2004. ZFIN Direct Data Submission. http://zfin.org

Vuocolo, T., Byrne, K., White, J., McWilliam, S., Reverter, A., Cockett, N. E., & Tellam, R. L. (2007). Identification of a gene network contributing to hypertrophy in callipyge skeletal muscle. *Physiological Genomics*, *28(3)*, *253-272*, *28*, 253–272. https://doi.org/10.1152/physiolgenomics.00121.2006

Wang, K., Li, M., & Hakonarson, H. (2010). ANNOVAR: Functional annotation of genetic variants from high-throughput sequencing data. *Nucleic Acids Research*, *38*(16):e164.

SUPPORTING INFORMATION

Additional supporting information may be found online in the Supporting Information section.

How to cite this article: Ain NU, Muhammad N, Dianatpour M, et al. Biallelic *TMEM251* variants in patients with severe skeletal dysplasia and extreme short stature. *Human Mutation*. 2021;42:89–101. https://doi.org/10.1002/humu.24139